

Migration mechanism for oversized solutes in cubic lattices: The case of yttrium in ironJean-Louis Bocquet,^{1,*} Caroline Barouh,² and Chu-Chun Fu²¹*CMLA, ENS Cachan, CNRS, Université Paris-Saclay, 94235 Cachan, France*²*DEN-Service de Recherches de Métallurgie Physique, CEA, Université Paris-Saclay, F-91191, Gif-sur-Yvette, France*

(Received 16 November 2016; revised manuscript received 7 April 2017; published 12 June 2017)

Substitutional solutes in metals generally diffuse by successive exchanges with vacancies, that is, via the so called vacancy mechanism. However, recent density functional theory (DFT) calculations predicted an atypical behavior for the oversized solute atoms (OSAs) in bcc and fcc iron. These solutes exhibit a very strong attraction with a nearby vacancy (V) at a first neighbor (1nn) distance. The attraction is so large that the 1nn OSA-V pair is no longer stable and relaxes spontaneously towards a new configuration where the OSA sits in the middle of the two half-vacancies (V/2). As a consequence, the diffusion of OSAs cannot be described by the standard vacancy mechanism. A new migration mechanism with a new formulation of correlation effects is required. The present study rests on a revised expression of the diffusion coefficient of the OSAs in bcc and fcc lattices, which introduces the concept of macrojumps. The formalism is applied presently to the case of yttrium (Y: a principal alloying element of advanced steels) in iron, using DFT data. But it is directly transferable to other OSAs in cubic metal lattices. At variance with the standard substitutional solutes, the Y atom is found to diffuse more rapidly than iron at all temperatures by orders of magnitude in the two cubic-Fe structures. This finding is opposite to the recent common belief that yttrium is a slow diffusing species in Fe alloys, based on experimental evidences. Several suggestions are proposed to solve this apparent inconsistency.

DOI: [10.1103/PhysRevB.95.214108](https://doi.org/10.1103/PhysRevB.95.214108)**I. INTRODUCTION**

Diffusion of solutes in solids plays a crucial role controlling a large variety of kinetic processes, such as precipitation, segregation to surfaces, dislocations and grain boundaries, etc. Recently, significant advances in predicting diffusion properties of solutes in metals have been achieved, from both modeling and atomistic simulation viewpoints [1–4], in particular from a more accurate description of correlation effects including solute-vacancy interactions beyond the first neighbor shells in various lattice structures (cubic [5], hexagonal [6], arbitrary lattice structure [7]) up to a thorough evaluation of phenomenological coefficients in dilute alloys [8]. But, beyond the standard vacancy mechanism, an exact and rigorous formalism for various atypical substitutional-solute diffusion is still missing.

For instance, first-principles calculations predicted recently that oversized solute atoms (OSAs) are dissolved as substitutional species in bcc and fcc iron. These OSAs include the transition metal elements (TM) at the beginning of the series (Sc, Y, Lu, Zr, and Hf) due to their big atomic size, compared with the host atom [9]. Also, the noble-gas elements can behave as OSAs in a TM lattice, because of the strong repulsion with the host atoms which creates a large effective solute volume [10,11]. As expected, there is a strong attraction of the OSAs with a nearby vacancy (V): for some of them it is so large that a 1nn OSA-V pair is no longer stable and relaxes spontaneously towards a new configuration where the OSA sits in the middle of the bond, the two ends of which are decorated with two half-vacancies (V/2) [1–3,10–13]. It is worth mentioning that the same type of complex was reported earlier for cadmium in silicon and germanium [14], and for helium in bcc iron [10]; it is also the case for yttrium in iron, as presented below. It is clear

that this new feature cannot be captured by today's existing diffusion formalisms and that the standard expressions for the diffusion coefficient and correlation factor cannot be used.

The oversized solutes can act as important alloying elements in advanced steels, which is the case of yttrium in ODS (oxide dispersion strengthened) steels. The ODS steels are of paramount importance in the future design of fusion devices, due to their exceptionally high resistance to creep: the pinning of dislocations is obtained thanks to a very high density of small immobile precipitates [15]. Among the possible alternate candidates [16], mixed yttrium-titanium oxides still occupy the pole position: they have been the subject of a large number of mainly experimental studies [17–22], the main effect of Ti being a decrease of the size of Y-Ti-O nanoscale clusters or precipitates [23–25], and also theoretical studies mixing first-principle calculations [26–32] and numerical simulations [18,33–35]. The fabrication of such alloys with a fine dispersion of Y-Ti-O nanoclusters or precipitates is, up to now, mainly done by a mechanical alloying of nanopowders mixing Y₂O₃ oxide with the iron-based matrix, with Ti as an additional impurity. At the end of the process the original Y₂O₃ oxides are no longer detectable, which is interpreted as a complete dissolution of Y and O in the lattice of the base matrix. The crucial step is then the annealing of the mixture at a high temperature in order to produce the small precipitates which are desired. The success of this complex nucleation-growth-coarsening process rests on basic key mechanisms, among which the yttrium diffusivity is one of importance. Since to our knowledge, no direct measurement of yttrium diffusivity through tracer technique has ever been reported [36], the only way out was to evaluate at best the diffusion coefficient at work in the precipitation process described above. This was done experimentally by Alinger [18,37] who proposed a diffusivity having a very high activation energy equal to 3.1 eV; kinetic Monte Carlo simulations performed afterwards could reproduce the experimental results (precipitate density and

*jean-louis.bocquet@cmla.ens-cachan.fr

size) with these experimentally deduced diffusion coefficients [33,34]. But the fabrication process incorporates a large supersaturation of dislocations, grain boundaries, vacancies, and oxygen. Due to a known strong trapping of Y atoms by the structural defects and by O atoms, such an experiment can only yield at best an environment-dependent effective value for the Y diffusivity, while giving no information on the intrinsic transport mechanism of yttrium and its diffusion coefficient.

The present contribution proposes a new variant of the vacancy mechanism for an exact determination of the OSA transport, which takes into account the existence of the $V/2 + \text{OSA} + V/2$ complex. The chemical species of the OSA will be denoted by B for generality and B^* will stand for a tagged atom of the B species, also called a tracer for short.

The first section sums up the theoretical analysis and recalls the analytical expressions to be used for the solute diffusion coefficient D_{B^*} and for the correlation factor f_B in the bcc and fcc lattices. In the second section we apply the new approach to yttrium diffusivity in bcc and fcc iron. Density functional theory calculations provide the atomic ingredients entering the diffusion coefficients, i.e., the solute-vacancy interactions, together with the migration barriers in the vicinity of the OSA. The variation with temperature of the corresponding diffusion coefficient and correlation factor is presented. Also, we discuss the implications of the results in the light of recent experimental and simulation results. Finally, conclusions are given in the third section.

II. THE NEW MIGRATION MECHANISM: A MODIFIED FORMULATION OF TRACER DIFFUSIVITY AND CORRELATION FACTOR

In the course of the new migration path, the tracer B^* occupies alternatively regular lattice sites as well as interstitial sites located at the middle of nearest neighbor bonds (denoted afterwards as intermediate sites). The analysis must then take this new feature into account in order to calculate correctly the mean square displacement. The migration mechanism is therefore a two-step process which can be described as follows:

(1) The 1nn neighbor vectors are denoted by $\{\omega_i\}$ (with length ω); the tracer B^* sits initially on the origin [Figs. 1(a) and 2(a)]; let us assume that a vacancy V jumps from some site R_{init} with $R_{\text{init}} \subset \{\omega_i + \omega_j\}$ belonging to more distant shells than the first neighbor one ($|R_{\text{init}}| > \omega$) towards a 1nn neighbor site of B^* , say ω_{i_0} [Figs. 1(a) and 2(a)]. Then the tracer B^* slides without any activation barrier towards the intermediate site $\lambda_{i_0} = \omega_{i_0}/2$ while the vacancy splits into two halves located on $r = 0$ and $r = \omega_{i_0}$ [Figs. 1(b) and 2(b)]. This is the first step of the diffusion process which ends up by the formation of a complex denoted $(V/2 + \text{OSA} + V/2)$ to remember that only one unoccupied vacancy was present before the formation of the complex.

(2) The second step of the diffusion process happens then:

(i) either the half-vacancy on ω_{i_0} jumps back towards one of its first neighbors $\omega_{i_0} + \omega_j$ (with $\omega_{i_0} + \omega_j \neq 0$) while repelling simultaneously the tracer B^* on the center of the cubic cell, in which case the net displacement of B^* is equal to zero;

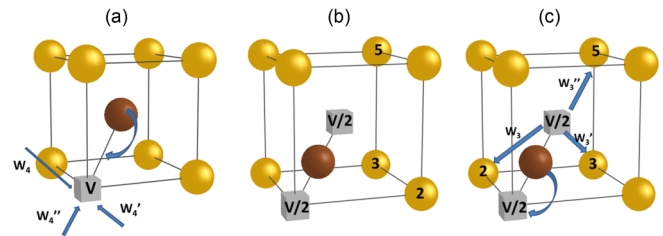


FIG. 1. OSA diffusion path including the formation and the dissociation of the $V/2 + \text{OSA} + V/2$ complex in a bcc lattice. The dark brown and the light spheres represent, respectively, the OSA and the host atoms. The cubes denote the vacant sites. The numbers on the atoms indicate the coordination shell with respect to the OSA. (a) Formation: various arrival paths for the vacancy; the OSA relaxes to the midpoint of the bond (curved arrow); (b) stable configuration of the complex; and (c) various dissociation paths: the OSA relaxes toward a new lattice site (curved arrow).

(ii) or the half-vacancy located on $r = 0$ jumps towards one of its first neighbors ω_{i_1} (with $\omega_{i_1} \neq \omega_{i_0}$) while rejecting simultaneously the B^* atom on site ω_{i_0} , in which case the net displacement of B^* is equal to ω_{i_0} [Figs. 1(c) and 2(c)].

The net displacement of B^* from a lattice site to a neighboring lattice site is called a macrojump; it becomes the new elemental displacement of the random walk.

This picture holds for both bcc and fcc lattices. An additional migration path must be envisaged because the pseudodivacancy (made of two half-vacancies) can also migrate as a whole. In the fcc lattice, it migrates while keeping its 1nn configuration: the tracer B^* is carried from one intermediate site to another, as symbolically sketched in Fig. 3, where the arrows denote the net displacements of the moving species. In the bcc lattice, the divacancy moves while adopting temporarily a 2 nn metastable configuration: it was shown previously that He was carried in this way in bcc iron [10].

Rigid-lattice atomic Monte Carlo simulations are often employed for studying diffusion and other kinetic processes (precipitation, ordering, etc.). For instance, it is worth mentioning that previous kinetic Monte Carlo simulations dealing with Y in bcc iron systems did not take into account the existence of this complex and assigned to yttrium diffusivity an effective value which is fitted on experimental precipitation kinetics [34]. If Monte Carlo simulations taking this effect into account appear as conceivable, they would have however to overcome a difficult problem of vacancy trapping in the close vicinity of the OSA: the existence of a deep attractive well induces

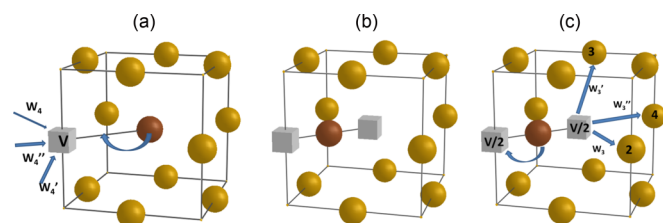


FIG. 2. OSA diffusion path including the formation and the dissociation of the $V/2 + \text{OSA} + V/2$ complex in a fcc lattice (same description as Fig. 1).

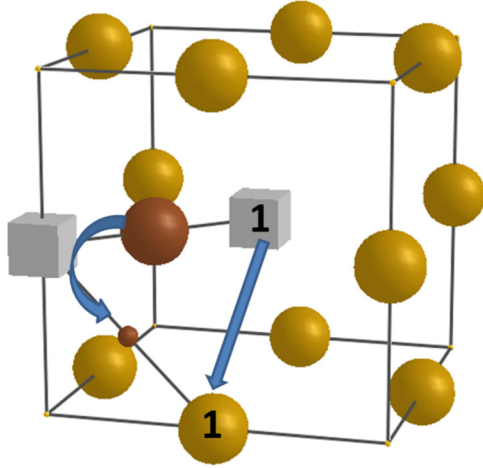


FIG. 3. Nondissociative jump of the $V/2 + \text{OSA} + V/2$ complex in a fcc lattice. The arrows denote the net displacement of the two species, from the initial positions to the final ones in the forefront lattice plane. For the OSA (brown sphere), the curved arrow means that the actual displacement passes through the substitutional site before relaxing towards its final position

a large number of flickering events which produce no net displacement and are highly time consuming, especially at low temperatures. Indeed, in such systems exhibiting a large disparity of frequencies, the brute force approach will become ineffectual at rather low temperatures and the recourse to specialized detrapping algorithms will therefore be mandatory to reach a sufficient statistical accuracy [38].

This is the reason why the present paper directs its effort on an exact modeling which starts from the detailed vacancy jump frequencies of the vacancy around the OSA obtained through first-principles calculations, while including the role of the complex in the migration process. The subsections below give the theoretical background and analysis of this variant of the vacancy mechanism. To focus mainly on the physical processes, only a synthetic summary is provided: all the technical details of the calculation are reported in a dedicated arXiv deposit [39].

A. Calculating the mean square displacement of a tagged atom

The diffusion coefficient of a tracer B^* in infinite dilution is related to its mean square displacement $\langle R^2(t) \rangle$ during a time interval t by the Einstein formula $D_{B^*} = \lim_{t \rightarrow \infty} \langle R^2(t) \rangle / 6t$, where the displacement is the result of all the jumps performed with a large number of distinct defects. These jumps can however be considered as:

(1) bunched in space: the number of jumps performed with only one vacancy is small (hardly larger than unity in 3D walks [40]) resulting in an overall displacement of a few lattice parameters only;

(2) bunched in time: the total vacancy concentration C_{V0} is small and the time interval separating the arrival of two different vacancies on the tracer is large compared to the time spent by one given vacancy in its vicinity. This implies that, on average, a vacancy labeled k will arrive in the neighborhood of the tracer only a long time after the vacancy labeled $k - 1$

definitely escaped after completion of its exchanges with the tracer.

The collection of solute jumps performed with the same vacancy can thus be gathered together into what is called an encounter [41]. The average time interval which separates the successive arrivals of two different vacancies in the neighborhood of the tracer B^* is denoted by Δt_{Enc} ; in other words it is nothing but the duration allotted to an encounter. Because the vacancy concentration is very low, these encounters do not noticeably overlap: their contributions can be considered as independent from one another and additive. This is the reason why the general formula above can be replaced by

$$D_{B^*} = \langle R^2 \rangle_{\text{Enc}} / 6\Delta t_{\text{Enc}}, \quad (1)$$

where $\langle R^2 \rangle_{\text{Enc}}$ is the mean square displacement of the tracer B^* during one encounter.

The encounter starts at time zero, when the tracer B^* , which was previously located on a substitutional site (denoted S), is pushed onto an intermediate site (denoted I), by a vacancy which it never encountered before, at a frequency denoted by Γ_{SI} . The possible vectors $\{\lambda_i\} = \{\omega_i/2\}$ for this $S \rightarrow I$ jump are collinear with the first neighbor vectors $\{\omega_i\}$ and their length is denoted by $\lambda = \omega/2$. Then the tracer atom B^* comes back onto a lattice site through an $I \rightarrow S$ jump of length λ , while expelling the vacancy on some neighboring site, at a frequency denoted by Γ_{IS} . This set of elementary displacements ($S \rightarrow I + I \rightarrow S$) which carries B^* from a regular lattice site to a regular lattice site is the macrojump introduced above. After this first macrojump, the tracer can initiate a second one thanks to the same vacancy with a probability P (strictly smaller than unity for a 3D walk [40]), a third macrojump with a probability P^2 , etc. Finally the vacancy will escape definitely to infinity or will be absorbed by a sink, which puts an end to the encounter.

The calculation of the mean square displacement of the tracer requires the introduction of probability functions SI and IS attached to $S \rightarrow I$ and $I \rightarrow S$ jump, respectively, and consists of establishing recurrence relations between them: for instance the tracer B^* reaches a site r through the $I \rightarrow S$ jump number n only if it has reached the intermediate site of a bond having one end on r through the $S \rightarrow I$ jump number $n - 1$. The mean square displacement corresponding to the encounter is expressed thanks to the second order moment of those functions which bring the tagged atom back onto a substitutional site, i.e., the IS ones [39]. Summing the recurrence equations over n from 1 to ∞ yields the desired moments. Hence the final expression:

$$\langle R^2 \rangle_{\text{Enc}} = \frac{\omega^2}{2(1 - P)} (1 + Q^{\text{bcc}}), \quad (2)$$

where P is the total probability of performing a $S \rightarrow I$ jump after an $I \rightarrow S$ one with the same vacancy, Q^{bcc} is the average cosine between an $I \rightarrow S$ jump vector and the next $S \rightarrow I$ one in the bcc lattice. The average number of macrojumps in an encounter is given by $1 + P + P^2 + \dots = (1 - P)^{-1}$. The mean square length of a macrojump is obtained thanks to Eq. (2) while setting $P = Q = 0$, which yields $\langle R^2 \rangle_{\text{MJ}} = \omega^2/2$. The mean square displacement produced by $(1 - P)^{-1}$ macrojumps is $\langle R^2 \rangle_{\text{rand}} = \langle R^2 \rangle_{\text{MJ}} (1 - P)^{-1}$ and the

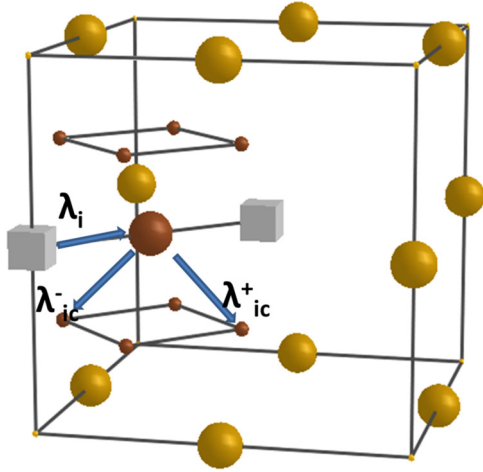


FIG. 4. Jump vectors for the OSA from an intermediate site to its eight neighbors in a fcc lattice; light spheres stand for fcc lattice sites; big and small brown spheres stand for intermediate sites.

correlation factor is by definition given by the ratio

$$f_B = \langle R^2 \rangle_{\text{Enc}} / \langle R^2 \rangle_{\text{rand}} = 1 + Q^{\text{bcc}}. \quad (3)$$

In this transport mechanism, the only correlation effect takes place between an $I \rightarrow S$ jump and the $S \rightarrow I$ one belonging to the next macrojump.

For a fcc lattice, the recurrence equations must be modified in order to take into account the additional $I \rightarrow I$ jump (Fig. 3) of frequency W_{II} : indeed, a tracer B^* sitting on an intermediate site can jump either toward a lattice site at a frequency W_{IS} (two possibilities) or toward another interstitial site at a frequency W_{II} (eight possibilities), as described in Fig. 4.

It can be shown that the II functions associated with this additional type of jump can be eliminated at the benefit of the IS ones [39]. As before the second order moments of the IS functions yield the desired result:

$$\langle R^2 \rangle_{\text{Enc}} = \frac{(1 + 2\alpha)\omega^2}{8\alpha(1 - P)} \left(1 + \frac{4\alpha}{1 + 2\alpha} Q^{\text{fcc}} \right), \quad (4)$$

where $2\alpha = \Gamma_{IS}/(\Gamma_{IS} + 8W_{II})$ and Q^{fcc} is the average cosine for the fcc lattice.

The mean square length of the macrojump is no longer constant but depends on the temperature through the frequency ratio 2α :

$$\langle R^2 \rangle_{\text{MJ}} = \omega^2(1 + 2\alpha)/8\alpha, \quad (5)$$

and the correlation factor is defined as above by

$$f_B = \frac{\langle R^2 \rangle_{\text{Enc}}}{\langle R^2 \rangle_{\text{Rand}}} = 1 + \frac{4\alpha}{1 + 2\alpha} Q^{\text{fcc}}. \quad (6)$$

The smaller α , the larger the length of a macrojump, and the larger the displacement during an encounter. As expected intuitively, the correlation factor becomes close to unity when the tracer B^* migrates mainly from an intermediate site to another without passing through a lattice site, a situation which mimics in a close way a direct interstitial mechanism.

B. Calculating the time duration for an encounter

Let us set the reference state of the energy as the crystal containing a tracer atom B^* on the origin and a noninteracting vacancy far apart in the bulk. The vacancy concentration in the bulk is denoted by C_{V0} and that at closer distances $C_{Vi} = C_{V0}e^{\beta E_i}$, where E_i is the vacancy-solute binding energy when the vacancy sits on the i th neighbor shell of the tracer ($E_i > 0$ for an attraction and $E_i < 0$ for a repulsion). Assuming an isotropic interaction, the jump frequency $W_{Ri \rightarrow Rj}$ of the vacancy from a lattice site R_i to a neighbor site R_j depends only on the neighbor shells sites R_i and R_j belong to. The notation $W_{Ri \rightarrow Rj}$ can thus be replaced by $W_{i \rightarrow j}^{\text{shell}}$, where the subscripts i and j stand for a shell index.

The macrojump is made of two steps in series: the passage from S to I site at a frequency Γ_{SI} is carried out by a vacancy jumping from R_{init} onto a site of the first neighbor shell of B^* ; the return on a substitutional site at the frequency Γ_{IS} is carried out when the vacancy (at any of the two ends of the complex) jumps back on a lattice site which belongs to $\{R_{\text{init}}\}$.

Γ_{SI} is the total jump frequency of a vacancy towards a first neighbor site of the atom B^* which sits on a lattice site. The sites R_{init} it starts from belong to more distant shells (labeled j) than the first one and the vacancy jump frequencies from shell j to shell 1 are named $W_{j \rightarrow 1}^{\text{shell}}$ ($j = 2, 3, 5$ for the bcc lattice, $j = 2, 3, 4$ for the fcc lattice). The probability of finding a vacancy on shell j is by definition its atomic concentration C_{Vj} and the frequency Γ_{SI} is thus expressed as

$$\begin{aligned} \Gamma_{SI} &= z \sum_{jV1} \text{nbond}_{1 \rightarrow j} C_{Vj} W_{j \rightarrow 1}^{\text{shell}} \\ &= z C_{V0} \sum_{jV1} \text{nbond}_{1 \rightarrow j} e^{-\beta E_j} W_{j \rightarrow 1}^{\text{shell}}, \end{aligned} \quad (7)$$

where z is the number of first neighbors; the summation \sum_{jV1} runs on the shells j which can be reached from the first shell through one jump; and $\text{nbond}_{1 \rightarrow j}$ is the number of bonds connecting a given site of the first shell to sites of the j th shell.

For the bcc lattice, using a standard notation for the frequencies which control the formation or the dissociation of the complex:

$$\begin{aligned} \text{nbond}_{1 \rightarrow 2} &= 3, & \text{nbond}_{1 \rightarrow 3} &= 3, & \text{nbond}_{1 \rightarrow 5} &= 1, \\ \Gamma_{SI} &= 8C_{V0}(3e^{\beta E_2} W_4 + 3e^{\beta E_3} W'_4 + e^{\beta E_5} W''_4), & W_{IS} &= \\ &= 3W_3 + 3W'_3 + W''_3, & \text{and } \Gamma_{IS} &= 2W_{IS} = 2(3W_3 + 3W'_3 + W''_3). \end{aligned}$$

Since the jumps $S \rightarrow I + I \rightarrow S$ are performed in series, their delays are additive:

$$\Delta t_{\text{MJ}} = (\Gamma_{SI})^{-1} + (\Gamma_{IS})^{-1}.$$

The frequency attached to a macrojump is thus defined as

$$\Gamma_{\text{MJ}} = (\Delta t_{\text{MJ}})^{-1} = \Gamma_{SI}\Gamma_{IS}/(\Gamma_{SI} + \Gamma_{IS}). \quad (8)$$

The duration of an encounter made of $(1 - P)^{-1}$ macrojumps is then $\Delta t_{\text{Enc}} = (1 - P)^{-1}\Delta t_{\text{MJ}}$ and the tracer diffusion coefficient is finally expressed as

$$D_{B^*} = \frac{\langle R^2 \rangle_{\text{Enc}}}{6\Delta t_{\text{Enc}}} = \frac{1}{6}\Gamma_{\text{MJ}} \frac{\omega^2}{2} (1 + Q^{\text{bcc}}). \quad (9)$$

For the fcc lattice:

$$\text{nbond}_{1 \rightarrow 2} = 2, \quad \text{nbond}_{1 \rightarrow 3} = 4, \quad \text{nbond}_{1 \rightarrow 4} = 1, \\ \Gamma_{\text{SI}} = 12C_{V0}(2e^{\beta E_2} W_4 + 4e^{\beta E_3} W'_4 + e^{\beta E_4} W''_4), \quad W_{\text{IS}} = \\ 2W_3 + 4W'_3 + W''_3, \text{ and } \Gamma_{\text{IS}} = 2W_{\text{IS}} = 2(2W_3 + 4W'_3 + W''_3).$$

It can be shown that the time spent on intermediate sites does not depend on the jump frequency W_{II} [39] and that the tracer diffusion coefficient is expressed as

$$D_{B^*} = \frac{\langle R^2 \rangle_{\text{Enc}}}{6\Delta t_{\text{Enc}}} = \frac{1}{6} \Gamma_{\text{MJ}} \frac{(1 + 2\alpha)\omega^2}{8\alpha} \left(1 + \frac{4\alpha Q^{\text{fcc}}}{1 + 2\alpha} \right). \quad (10)$$

C. Calculation of the correlation factor

The value of the correlation effect rests on the above-mentioned average cosine Q^{bcc} and Q^{fcc} between successive macrojumps in the two lattice structures.

After the completion of a macrojump, the OSA is repelled onto the origin and the vacancy sits on a lattice site belonging to the set $\{R_{\text{init}}\}$. The general method consists of solving the diffusion problem corresponding to a vacancy starting from any site of $\{R_{\text{init}}\}$ and coming back on any site of $\{R_{\text{init}}\}$ while avoiding the origin: the average cosine is nothing but the product of the time integral of the return probabilities of the vacancy on the arrival sites and the jump frequency which pushes the OSA on an intermediate site. Summing the contribution of all possible vacancy trajectories made of an arbitrary number of jumps is performed with a Fourier transform. Summing the probabilities over time is easily done with a Laplace transform. Denoting the probability of finding the vacancy at a regular lattice site r_i at time t by $L(r_i, t)$, its Laplace transform is given by $LL(r_i, p) = \int_0^\infty e^{-pt} L(r_i, t) dt$ and the time integral is defined by $p_i^{\text{ret}} = \int_0^\infty L(r_i, t) dt$. The latter is nothing but the value of the Laplace transform for $p = 0$, i.e., $LL(r_i, p)|_{p=0}$. Hence the use of a double Laplace and Fourier transform of the transport equation for the vacancy, which yields the desired quantities [5,39]. The return probabilities take into account all the jump frequencies $W_{i \rightarrow j}^{\text{shell}}$ which are different from the jump frequency W_O in the bulk. In the general case, their analytical expressions are out of reach for interactions ranging beyond the first neighbor shell; their values can however be calculated exactly as the solution of a linear system. The coefficients of this system combine the above modified frequencies with quantities which depend only on the random walk propagator for the lattice structure under study, i.e., lattice integrals calculated in the first Brillouin zone [5,39].

For the bcc lattice, the average cosine is found to be equal to

$$Q^{\text{bcc}} = -4p_2^{\text{ret}} W_4 - 8p_3^{\text{ret}} W'_4 - 4p_5^{\text{ret}} W''_4, \quad (11)$$

where p_i^{ret} is the time-integrated probability on a lattice site belonging to neighbor shell i .

For the fcc lattice, the average cosine is found to be equal to

$$Q^{\text{fcc}} = -4p_2^{\text{ret}} W_4 - 8(p_{3,1}^{\text{ret}} + p_{3,2}^{\text{ret}}) W'_4 - 4p_4^{\text{ret}} W''_4, \quad (12)$$

where the time-integrated probabilities on the sites of the third neighbor shell $p_{3,1}^{\text{ret}}$ and $p_{3,2}^{\text{ret}}$ have to be distinguished for symmetry considerations.

III. THE CASE OF YTTRIUM IN BCC AND FCC IRON

A. Vacancy-yttrium interactions and migration barriers from first principles

We have investigated the diffusion of yttrium, as a representative OSA, in the bcc and the fcc iron lattices. We confirm the formation of the very stable $V/2 + Y + V/2$ complex in both bcc and fcc iron, as proposed by previous DFT studies [11,13]. First-principles calculations within the density functional theory (DFT) framework were performed using the SIESTA code [42]. They provide key data for determining the solute diffusion coefficients, that is, the solute-vacancy interaction energies and the barriers for vacancy jumps, as functions of the solute-vacancy separation distance. The SIESTA approach has already been extensively applied for predicting energetics and migration properties of solutes in Fe systems [3,10,43–45].

The calculations were spin polarized in the case of yttrium in bcc iron, in order to account for the ferromagnetism. The fcc iron phase exhibits spin spirals at the ground state, and it is stabilized with the paramagnetic state above the α - γ transition temperature. Simulating the complex magnetic configurations including magnetic disorder is out of the scope of the present work. For simplicity, we only assumed a nonmagnetic state for fcc iron.

We adopted the generalized gradient approximation (GGA) with the Perdew-Burke-Ernzerhof (PBE) exchange-correlation functional [46]. Core electrons were replaced by norm-conserving pseudopotentials. Valence electrons were described by linear combinations of numerical pseudoatomic orbitals. The pseudopotential and the basis set for Fe are the same as in Refs. [3,45], with a pseudopotential cut-off radius of 1.15 Å and a basis set of ten localized functions per atom. The cut-off radii for the pseudopotentials of yttrium are set to 1.37, 0.76, and 0.82 Å, respectively for the $5s$, $4p$, and $4d$ states. The basis set of each Y atom consists of two strictly localized functions for the $5s$ states, three for the $4p$, and five for the $4d$ states. The cut-off radii are respectively 4.14, 2.74, and 3.65 Å. Three functions for the $5p$ states are also included as polarized orbitals in order to increase angular flexibility. The charge density is represented on a regular 0.067 Å width grid in the real space.

A cubic supercell of 250-atom sites with a $2 \times 2 \times 2$ k -point grid were used for the case of bcc-Fe, and a 256-sites supercell with $3 \times 3 \times 3$ k grid were employed for the fcc-Fe. The Methfessel-Paxton broadening scheme with a 0.3 eV width was used [47]. We have checked that the obtained binding energies and migration barriers are well converged with respect to the supercell size and the k -point grid. The estimated uncertainties are all smaller than 0.05 eV.

In all the cases, a system containing a solute and/or a vacancy was relaxed by optimizing the atomic positions keeping the volume of the supercell constant as in the defect-free system (constant-volume approximation). The convergence criterion was set to be 0.04 eV/Å for the residual forces.

The binding energy between a yttrium solute and a vacancy is determined as

$$E_B = E[(N-1)\text{Fe}] + E[(N-1)\text{Fe}, Y] \\ - E(N\text{Fe}) - E[(N-2)\text{Fe}, Y], \quad (13)$$

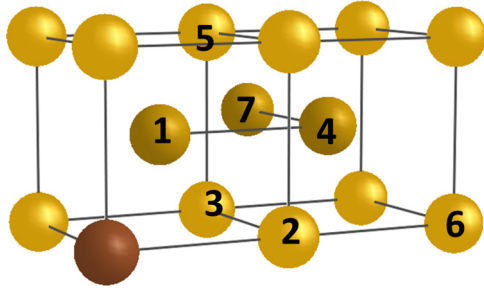


FIG. 5. Definition of neighborhoods in the bcc lattice. The yttrium atom (brown sphere) sits on the lower left site of the forefront lattice plane.

where $E[(N-1)\text{Fe}]$, $E[(N-1)\text{Fe}, \text{Y}]$, and $E[(N-2)\text{Fe}, \text{Y}]$ are the total energy of the system containing, respectively, a vacancy (V), a substitutional Y atom, and a vacancy near a substitutional Y. $E(N\text{Fe})$ denotes the total energy of a perfect bcc or fcc iron lattice, with $N\text{Fe}$ atoms. Here a positive binding energy means attraction.

Migration barriers and paths were calculated using the drag method [48], that is, the atomic positions are constrained to relax in a hyperplane perpendicular to the vector connecting the initial and final positions. This method has shown to provide results with satisfactory precision for calculating migration barriers in solid systems [3,10,43–45,49–51].

B. Application to the case of Y in bcc iron

Due to the high technological interest of the advanced ODS steels, properties of yttrium in a bcc-iron lattice has been investigated by various authors. It is worth noticing that the existence of the $V/2 + Y + V/2$ complex was not always recognized previously. A tiny but positive migration barrier (0.02 eV) for the jump of an yttrium atom toward a first neighbor vacancy was reported, based on *ab initio* calculations, which apparently prevents the formation of the complex [52]. But the same authors also mentioned that in such a configuration, the yttrium atom significantly shifts towards the incoming vacancy. The positive barrier allowed the authors to calculate the diffusion coefficient with the expressions of the standard model for the bcc structure. To our knowledge, this result was however never reproduced later on, neither with the

same *ab initio* code [11], nor with other DFT implementations [12]. Therefore, unless future contradictory reports, we take the existence of the complex for granted.

In order to study the Y diffusion with our new model, we have adopted a vacancy formation energy of 2.12 eV, based on our DFT calculations, and a vacancy formation entropy of $4.08 k_B$ according to previous DFT estimations [53]. For simplicity, the pre-exponential term is taken equal to the Debye frequency 10^{13}s^{-1} for all jump frequencies. The vacancy migration energy in the bulk, as obtained by DFT, is equal to 0.69 eV. The lattice parameter found is $2.87 \times 10^{-10}\text{m}$.

The relative positions of the yttrium atom and of the vacancy are depicted in Fig. 5. The values of interaction energies and migration barriers are gathered in Table I. The diffusion coefficient of a tracer iron atom is expressed as $D_{\text{Fe}^*}^{\text{bcc}} = \frac{4}{3} C_{V0} W_0 f_0 \omega^2$, where the correlation factor f_0 is a constant which depends only on the geometry of the bcc lattice ($f_0 = 0.727$). The total activation energy for diffusion is the sum of the vacancy formation and migration energies.

The results of our calculation are displayed in Table II and Fig. 6. In spite of the complex migration mechanism, the Arrhenius plot does not exhibit any noticeable curvature over the explored temperature range. Because the correlation factor is a complicated function of the jump frequencies which are thermally activated, it has also an activation energy; in all the cases known up to now, this activation energy is much smaller than that for the diffusion jump itself, but it can be non-negligible. In the present case the effective activation energies coming from the f_Y^{exact} and $\Gamma_{\text{MJ}}^{\text{exact}}$ terms amount to 0.18 and 1.96 eV, respectively, yielding a total effective activation energy $E_{\text{act}}^{\text{exact}} = 2.14$ eV and a pre-exponential factor $D_0 = 2.4 \times 10^{-6} \text{m}^2 \text{s}^{-1}$.

Besides this exact calculation, a first approximate evaluation of yttrium diffusivity was recently proposed [12]. The approximation consists of ignoring the $1\text{nn} \leftrightarrow 5\text{nn}$ transitions (W_3', W_4') which leads to flicker events without producing any net transportation of the yttrium atom, as well as the $1\text{nn} \rightarrow 2\text{nn}$ transition (W_3, W_4) which requires too high an energy. Only the $1\text{nn} \rightarrow 3\text{nn}$ jump (frequency W_3') and the reverse jump (frequency W_4') are kept. At last, a constant correlation factor $f_Y^{\text{approx}} = 0.5$ was assumed: indeed, when sitting on a 3nn site after a W_3' jump, the vacancy has only two possibilities for an immediate return of equal probability:

TABLE I. Binding energies of the vacancy + OSA configurations at various distances in bcc iron and the migration barriers between the configurations, where i stands for i th neighbor shell of the yttrium atom (a positive sign means an attraction). Binding and migration energies are given in eV.

Vacancy on shell i	Binding energy	Jump toward shell j	Migration barrier for jump $W_{i \rightarrow j}^{\text{shell}}$	Migration barrier for jump $W_{j \rightarrow i}^{\text{shell}}$
1	+ 1.2	2	2.0	0.89
		3	1.22	0.16
		5	1.02	0.05
2	+ 0.09	4	0.69	0.61
		3	0.79	0.66
3	+ 0.14	7	0.83	0.69
		5	0.69	0.91
4	+ 0.01	6, 8, 9	0.70	0.69
		7, 10	0.91	0.69

TABLE II. Correlation factor, macrojump frequency (s^{-1}), and diffusion coefficient (m^2s^{-1}) for yttrium tracer in bcc iron. The exact result is compared with the approximation [12].

T (K)	f_Y^{exact}	$\Gamma_{\text{MJ}}^{\text{exact}}$	$D_{Y^*}^{\text{exact}}$	$D_{Y^*}^{\text{approx}}$
300	4.358×10^{-4}	1.213×10^{-17}	2.723×10^{-41}	1.576×10^{-41}
400	2.993×10^{-3}	1.719×10^{-9}	2.649×10^{-32}	1.041×10^{-32}
500	9.368×10^{-3}	1.356×10^{-4}	6.542×10^{-27}	2.038×10^{-27}
600	1.966×10^{-2}	2.545×10^{-1}	2.576×10^{-23}	6.875×10^{-24}
700	3.275×10^{-2}	5.650×10^1	9.526×10^{-21}	2.276×10^{-21}
800	4.720×10^{-2}	$3.306 \times 10^{+3}$	8.033×10^{-19}	1.767×10^{-19}
900	6.190×10^{-2}	$7.934 \times 10^{+4}$	2.528×10^{-17}	5.215×10^{-18}
1000	7.613×10^{-2}	$1.017 \times 10^{+6}$	3.985×10^{-16}	7.820×10^{-17}

the first cancels the macrojump and the second produces a macrojump length equal to the 1nn distance. The diffusion coefficient $D_{Y^*}^{\text{Barouh}}$ is then expressed by a single thermally activated term $D_O \exp[-E_{\text{act}}/(k_B T)]$, with $E_{\text{act}} = 2.10$ eV and $D_O = 3.0 \times 10^{-6} m^2 s^{-1}$.

Very interestingly, the resulting approximate diffusion coefficients are different from the exact values only by a factor ranging from 1.6 at the lower temperatures to 5.3 at the higher ones, thanks to the simple physical arguments considered above. This approximate model is actually a particular case of the called ‘‘one-shot’’ model, as detailed in the Appendix, where we demonstrate why this approximation works so well. The one-shot model consists of allowing the vacancy, after its dissociation from the OSA, to perform only one further jump for returning to a 1nn site of the OSA. Such approximation induces mechanically a nearly constant correlation factor close to 0.33 (which is not too far from the adopted value of 0.5), and this overestimated value of the correlation effect is fortuitously compensated by an underestimation of the macrojump frequency. Please note that the one-shot approximation gives simplified expressions for the diffusion coefficients and the correlation factors (Appendix). It is expected to give a reasonable estimation of diffusion coefficients as long as the vacancy-solute interaction is very strong at a 1nn separation,

with a rapid decrease with increasing separation distances, which is clearly the case of Y in bcc iron (Table I).

One additional comment is worth being made about the importance of correlation effects. It can be shown that the smallness of the correlation factor f_Y^{exact} is not implied by the existence of the vacancy + OSA complex and its intervention in the migration mechanism, but only by the particular set of vacancy jump frequencies around the yttrium atom. Indeed, in such a mechanism, the OSA occupies alternately the sites of the regular bcc lattice and the sites at the middle of first neighbor bonds. If this mechanism is considered independently of any energetic considerations by assuming that all jump frequencies are equal to a common value W_o , then the correlation factor is found equal to 0.761603 [39], that is, close to the value of the correlation factor for self-diffusion with a pure vacancy mechanism in the bcc structure.

The conclusion of this section points out the fact that the yttrium atom is definitely more rapid than the iron atom in the bcc structure, at the thermal vacancy regime.

This result is however at variance with the common belief that yttrium is a slow diffuser in bcc Fe. To our knowledge, the very high activation energy for Y relies on the only reported experiment-based Y diffusion coefficients, obtained by fitting to experimental small angle neutron scattering data in an ODS-FeCr alloy, using a classical nucleation-growth-coarsening model [37].

Some reasons can contribute to explain the low diffusivity of yttrium from the experiments:

(1) The introduction of yttrium into iron through mechanical alloying with yttrium oxide induces a large number of vacancies and oxygen atoms in supersaturation. DFT studies [12,49] showed that the binding energy of yttrium to vacancy and to vacancy clusters is high. Furthermore, if considering the migration of a complex as a unit, and adopting the effective migration energy E_m^{eff} of the cluster to be the largest barrier along the most probable migration path, as explained in Ref. [3], we found that the E_m^{eff} increases with n for YV_n clusters. For instance, the value calculated via the same DFT implementation as the present work for the YV complex is 1.22 eV, while that for YV₂ and YV₃ clusters are as high as 1.80 and 2.09 eV, respectively [12]. In addition, the dissociation energy of these clusters (via emission of a vacancy) also increases with the cluster size, for example, 1.89, 2.14, and 2.60 eV for YV, YV₂, and YV₃, respectively [12]. A vacancy supersaturation is therefore expected to favor the YV₂ and YV₃ clusters at

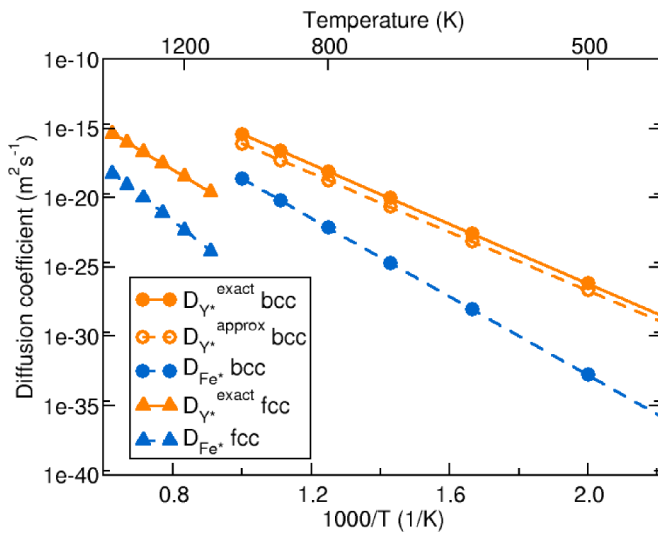


FIG. 6. Diffusion coefficients of yttrium and iron tracer in bcc and fcc iron resulting from the exact calculation or from the approximation given in Sec. III B.

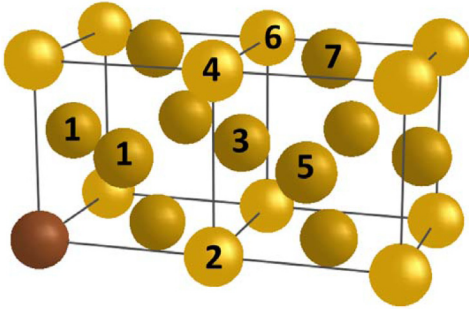


FIG. 7. Definition of neighborhoods in the fcc lattice. The yttrium atom (brown sphere) sits on the lower left site of the forefront lattice plane.

the expense of the most mobile YV, which can decrease the apparent diffusivity of yttrium by orders of magnitude.

(2) Also, there is as expected a strong oxygen-yttrium and oxygen-vacancy attraction [12,54,55]. The presence of oxygen induces the production of oxygen-vacancy clusters. Certain ones (the small OV_n) can be significantly mobile [55]. The strong attraction between yttrium, oxygen, and vacancies together with the high mobility of oxygen, vacancy, and their small clusters can lead to the formation of $V_n Y_m O_p$ clusters which are expected to be very stable but showing reduced mobility.

C. Application to the case of yttrium in fcc iron

In order to determine the tracer diffusion coefficients of Y in fcc iron, we have adopted a vacancy formation energy of 2.543 eV, based on our DFT calculations and a vacancy formation entropy of $2.0k_B$, which is a commonly accepted value for fcc metals [56]. For simplicity, the pre-exponential

term is taken equal to the Debye frequency 10^{13} s^{-1} for all jump frequencies. The vacancy migration energy in the bulk, as obtained by DFT, is equal to 1.34 eV. The lattice parameter found is $3.51 \times 10^{-10} \text{ m}$. The configurations which were calculated are depicted in Fig. 7; the associated yttrium-vacancy binding energies and the relevant migration barriers are gathered in Table III.

As above, the large attractive interaction energy between the yttrium atom and the vacancy is accompanied by small dissociation frequencies W_3, W_3', W_3'' and high re-association frequencies W_4, W_4', W_4'' . The additional feature is now the existence of the rotation frequency $W_{II} = W_I$ (Fig. 3). For this jump, the calculation shows that during the ascent of the migrating iron atom toward its saddle, the yttrium atom is progressively pushed back on its lattice site. During the descent towards the new equilibrium position, the yttrium atom relaxes again towards the new position of the moving vacancy at the end of the process. As a result, the rotation of the divacancy is accompanied by a net displacement of the yttrium atom from an intermediate site to a neighboring one, as described in Sec. I and schematically depicted in Fig. 3.

In Table IV are gathered the values of the calculated correlation factor f_Y^{exact} and yttrium diffusion coefficient D_{Y*}^{exact} , to be compared with the values of self-diffusion in fcc iron given by $D_{\text{Fe}*}^{\text{fcc}} = 2C_{V0}W_0f_0\omega^2$, with ($f_0 = 0.781$) as displayed in Fig. 6.

Correlation effects are still noticeable, but less marked than in the bcc structure and with a weaker temperature dependence. In the present case the impact of the rotation frequency $W_{II} = W_I$ is negligible, because of its large activation barrier (2.47 eV): the factor 2α remains very close to unity.

Once more, the smallness of the correlation factor is not linked to the migration mechanism as such but is mainly due to the high interaction energy at first neighbor distance, together

TABLE III. Binding energies of the vacancy + OSA configurations at various distances in the fcc lattice and the migration barriers between the configurations, where i stands for i th neighbor shell of the yttrium atom (a positive sign means an attraction). Binding and migration energies are given in eV.

Vacancy on shell i	Binding energy	Jump toward shell j	Migration barrier for jump $W_{i \rightarrow j}^{\text{shell}}$	Migration barrier for jump $W_{i \rightarrow i}^{\text{shell}}$
1	+1.32	1	2.47	2.47
		2	2.10	0.69
		3	1.72	0.54
		4	1.65	0.54
2	-0.09	3	1.25	1.48
		5	1.25	1.36
3	+0.14	3	1.48	1.48
		4	1.58	1.65
		5	1.25	1.13
		6	1.32	1.19
		7	1.29	1.22
4	+0.21	5	1.55	1.36
		7	1.24	1.10
		9	1.55	1.34
5	+0.02	5	1.36	1.36
		7	1.36	1.41
		8, 9, 10	1.36	1.34
6	+0.01	7	1.31	1.37
7	+0.07	7, 9, 10	1.41	1.34

TABLE IV. Correlation factor, macrojump frequency (s^{-1}), and tracer diffusion coefficient (m^2s^{-1}) for yttrium tracer in fcc iron.

T (K)	f_Y^{exact}	$\Gamma_{\text{MJ}}^{\text{exact}}$	$D_{Y^*}^{\text{exact}}$
1100	0.1664	1.782×10^2	2.538×10^{-20}
1200	0.1710	2.326×10^3	3.405×10^{-19}
1300	0.1754	2.047×10^4	3.074×10^{-18}
1400	0.1797	1.322×10^5	2.033×10^{-17}
1500	0.1841	6.655×10^5	1.049×10^{-16}
1600	0.1888	2.737×10^6	4.428×10^{-16}

with high re-association frequencies W_4, W_4', W_4'' , as in the bcc case. Please note that if a common value is assigned to all jump frequencies, the correlation factor for this mechanism is found equal to 0.787081, which is close to the value for the pure vacancy mechanism in the fcc structure [39].

At last, based on the present prediction, the yttrium atom diffuses more rapidly than iron also in the fcc phase at the thermal vacancy regime.

IV. CONCLUSIONS

At variance with standard substitutional solutes in a cubic lattice, an oversized solute atom (OSA) close to a vacancy can form a tightly bound complex, in which the solute sits in the middle of a first neighbor bond. This specific behavior has been theoretically predicted for various early series transition-metal elements and some noble gas atoms in both bcc and fcc iron lattices.

Since the diffusion of the OSAs cannot be carried out via the standard vacancy mechanism, the present study works out a new approach which includes a new mechanism for a quantitative determination of diffusion properties of the OSAs in bcc and fcc lattices. Splitting the OSA trajectory into encounters and macrojumps provides a simple way to define the quadratic displacement and the macrojump frequency. The theoretical results are applied to the case of yttrium diffusion in bcc and fcc iron, based on first-principles results as starting physical ingredients. Under thermal-vacancy conditions, yttrium is found to diffuse orders of magnitude faster than iron in the two structures. To the best of our knowledge, there is no tracer diffusion data available for Y in pure iron. The present result is opposite to previously reported Y diffusion coefficients deduced from experimental data in ODS-FeCr alloys. A significant amount of vacancies and oxygen atoms present in the experimental samples during the precipitation, which strongly binds to Y and slows down its diffusion, can be a plausible explanation of the apparent discrepancy.

The present modeling approach is directly transferable to other OSAs in cubic lattices, with the most probable corollary that those OSAs, which form tightly bound complexes with a vacancy, are most probably rapid diffusers in the thermal vacancy regime.

With the diffusion coefficients calculated in the present way, effective activation energies for the macrojumps can be derived, monitoring the transport of the OSA. These energies can be then used to parametrize Monte Carlo simulations with

a twofold advantage: the simulations will not need to include explicitly the intermediate sites in the rigid-lattice model, and will escape the penalty attached to the trapping-detrapping problem mentioned in the first section.

ACKNOWLEDGMENTS

J. L. Bocquet thanks the LRC-Méso (a joint laboratory formed by CMLA and CEA/DAM) for his support. The first-principles calculations were made using resources from DARI-GENCI within the Project No. A0010906020. This work was partially supported by the joint program ‘‘CPR ODISSEE’’ funded by AREVA, CEA, CNRS, EDF, and Mécachrome under Contract No. 070551.

APPENDIX: ONE-SHOT EVALUATION OF AVERAGE COSINE $Q_{1\text{shot}}^{\text{bcc}}$ IN THE BCC LATTICE

The one-shot approximation is rough and consists of allowing the vacancy, after its dissociation from the OSA, to perform only one further jump for returning close to the OSA.

Let us assume that the OSA is at site λ_{111} . When the half-vacancy at $\omega_{111} = 2\lambda_{111}$ dissociates from the OSA, the latter slips back to lattice site $r = 0$ with a jump $\lambda_{\bar{1}\bar{1}\bar{1}}$ parallel to $\omega_{\bar{1}\bar{1}\bar{1}}$. The vacancy pops up into seven parts on its seven possible neighbors with weights proportional to the dissociating frequencies and reaches:

(1) Three second neighbors of the origin at $\omega_{111} + \omega_{\bar{1}\bar{1}\bar{1}}, \omega_{111} + \omega_{\bar{1}\bar{1}\bar{1}}, \omega_{111} + \omega_{\bar{1}\bar{1}\bar{1}}$ with a relative probability $c_3 = W_3/(3W_3 + 3W_3' + W_3'')$ for each of them.

(2) Three third neighbors of the origin at $\omega_{111} + \omega_{\bar{1}\bar{1}\bar{1}}, \omega_{111} + \omega_{\bar{1}\bar{1}\bar{1}}, \omega_{111} + \omega_{\bar{1}\bar{1}\bar{1}}$ with a relative probability $c_3' = W_3'/(3W_3 + 3W_3' + W_3'')$ for each of them.

(3) One fifth neighbor of the origin at $r = 2\omega_{111}$ with a relative probability $c_3'' = W_3''/(3W_3 + 3W_3' + W_3'')$.

The vacancy is then allowed to perform one jump. We define the relative probabilities of occurrence for the association jumps: $p_4 = W_4/(4W_4 + 4W_5)$, $p_4' = W_4'/(2W_4' + 6W_0)$, $p_4'' = W_4''/(W_4'' + 7W_0)$, where W_5 is the standard name for the jump frequency from second to fourth neighbor shell.

The values of the corresponding cosine are calculated with respect to the direction $\omega_{\bar{1}\bar{1}\bar{1}}$ of the preceding $I \rightarrow S$ jump of the OSA. The probabilities that the vacancy comes back on a first neighbor site of the OSA are listed below in Table V. The multiplicative factor in the last column accounts for the

TABLE V. Contributions to the average cosine from the first returning jump.

Weight	Starting site	Arrival site	Rel. prob.	cos(θ)	Contribution to $Q_{1\text{shot}}^{\text{bcc}}$	\times factor
c_3	$\omega_{111} + \omega_{\bar{1}\bar{1}\bar{1}}$	ω_{111}	p_4	-1	$c_3[p_4(-1)]$	3
		$\omega_{\bar{1}\bar{1}\bar{1}}$ or $\omega_{\bar{1}\bar{1}\bar{1}}$	p_4	-1/3	$c_3[2p_4(-1/3)]$	
		$\omega_{\bar{1}\bar{1}\bar{1}}$	p_4	+1/3	$c_3[p_4(+1/3)]$	
c_3'	$\omega_{111} + \omega_{\bar{1}\bar{1}\bar{1}}$	ω_{111}	p_4'	-1	$c_3'[p_4'(-1)]$	3
		$\omega_{\bar{1}\bar{1}\bar{1}}$	p_4'	-1/3	$c_3'[p_4'(-1/3)]$	
c_3''	$2\omega_{111}$	ω_{111}	p_4''	-1	$c_3''[p_4''(-1)]$	1

TABLE VI. Comparison of the exact and approximate values of the correlation factor for OSA yttrium tracer in bcc iron.

T (K)	$f_{\text{OSA}^*}^{\text{exact}}$	$f_{\text{OSA}^*}^{\text{1shot}}$	$f_{\text{OSA}^*}^{\text{1shot+approx}}$	$\Gamma_{\text{MJ}}^{\text{approx}}$
300	4.356×10^{-4}	4.356×10^{-4}	0.3333	1.587×10^{-20}
400	2.993×10^{-3}	2.993×10^{-3}	0.3333	1.543×10^{-11}
500	9.368×10^{-3}	9.370×10^{-3}	0.3333	3.812×10^{-6}
600	1.966×10^{-2}	1.969×10^{-2}	0.3334	1.501×10^{-2}
700	3.275×10^{-2}	3.293×10^{-2}	0.3337	5.550
800	4.720×10^{-2}	4.787×10^{-2}	0.3342	$4.679 \times 10^{+2}$
900	6.190×10^{-2}	6.368×10^{-2}	0.3355	$1.471 \times 10^{+4}$
1000	7.613×10^{-2}	8.003×10^{-2}	0.3376	$2.314 \times 10^{+5}$

number of sites bringing the same contribution to the average cosine.

Summing up all the contributions gives the average cosine $Q_{\text{1shot}}^{\text{bcc}}$:

$$Q_{\text{1shot}}^{\text{bcc}} \approx -\frac{1}{3W_3 + 3W'_3 + W''_3} \times \left[\frac{4W_3W_4}{4W_4 + 4W_5} + \frac{4W'_3W'_4}{2W'_4 + 6W_0} + \frac{W''_3W''_4}{W''_4 + 7W_0} \right]. \quad (\text{A1})$$

This approximation is known to yield a returning probability always smaller—and a correlation factor always larger—

than the exact one since it neglects all the trajectories of the returning vacancy which are made of more jumps.

Applying these approximations to the case of yttrium in bcc iron ($\text{OSA} \equiv \text{Y}$) yields the values of the correlation factor $f_{\text{OSA}}^{\text{1shot}}$ displayed below in Table VI, assuming $W_5 = W_0$. Comparison with Table II shows that, although crude, the approximation retains most of the physics and yields a reasonable magnitude for the correlation factor over the whole range of temperature: as expected, the agreement deteriorates with increasing temperatures.

Then the approximation used in Ref. [12] is introduced: dropping of W_3, W'_3, W_4, W''_4 reduces the expressions of the average cosine and correlation factor to

$$Q_{\text{1shot+approx}}^{\text{bcc}} \approx -\frac{4W'_4}{3(2W'_4 + 6W_0)},$$

$$f_{\text{OSA}}^{\text{1shot+approx}} \approx \frac{W'_4 + 9W_0}{3W'_4 + 9W_0} = \frac{1}{3} + \frac{2W'_4}{3W'_4 + 9W_0}. \quad (\text{A2})$$

Table VI displays the values of $f_{\text{OSA}}^{\text{1shot+approx}}$ which are nearly constant and slightly larger than $1/3$. This is, after all, not too far from the value 0.5 retained originally by this author. Dropping W_3, W'_3, W_4, W''_4 in the expression of the macrojump frequency leads to the values $\Gamma_{\text{MJ}}^{\text{approx}}$ which are reported in Table VI. The comparison with Table II of the main section shows that the underestimation of the macrojump frequency $\Gamma_{\text{MJ}}^{\text{approx}}$ is practically compensated by the overestimation of the correlation factor $f_{\text{OSA}}^{\text{1shot+approx}}$; this explains the closeness of the approximated value with our own one, with the one-shot and with the physical approximation retained in Ref. [12].

-
- [1] L. Messina, M. Nastar, N. Sandberg, and P. Olsson, *Phys. Rev. B* **93**, 184302 (2016).
- [2] T. Schuler and M. Nastar, *Phys. Rev. B* **93**, 224101 (2016).
- [3] C. Barouh, T. Schuler, C. C. Fu, and T. Jourdan, *Phys. Rev. B* **92**, 104102 (2015).
- [4] S. Huang, D. L. Worthington, M. Asta, V. Ozolins, G. Ghosh, and P. K. Liaw, *Acta Mater.* **58**, 1982 (2010).
- [5] J. L. Bocquet, *Philos. Mag.* **94**, 3603 (2014).
- [6] A. R. Allnatt, I. V. Belova, and G. E. Murch, *Philos. Mag.* **94**, 2487 (2014).
- [7] R. Agarwal and D. R. Trinkle, *Phys. Rev. Lett.* **118**, 105901 (2017).
- [8] L. Messina, M. Nastar, T. Garnier, C. Domain, and P. Olsson, *Phys. Rev. B* **90**, 104203 (2014).
- [9] D. J. Hepburn, D. Ferguson, S. Gardner, and G. J. Ackland, *Phys. Rev. B* **88**, 024115 (2013).
- [10] C. C. Fu and F. Willaime, *Phys. Rev. B* **72**, 064117 (2005).
- [11] A. Claisse and P. Olsson, *Nucl. Instrum. Methods Phys. Res. B* **303**, 18 (2013).
- [12] C. Barouh, Ph.D. thesis, Université d'Orléans, France, 2015.
- [13] D. J. Hepburn, E. MacLeod, and G. J. Ackland, *Phys. Rev. B* **92**, 014110 (2015).
- [14] H. Höhler, N. Atodiresei, K. Schroeder, R. Zeller, and P. H. Dederichs, *Phys. Rev. B* **70**, 155313 (2004).
- [15] I.-S. Kim, J. D. Hunn, N. Hashimoto, D. L. Larson, P. J. Maziasz, K. Miyahara, and E. H. Lee, *J. Nucl. Mater.* **280**, 264 (2000).
- [16] J. Hoffmann, M. Rieth, R. Lindau, M. Klimenkov, A. Möslang, and H. R. Zschommler Sandim, *J. Nucl. Mater.* **442**, 444 (2013).
- [17] S. Ukai, M. Harada, H. Okada, M. Inoue, T. Nishida, and M. Fujiwara, *J. Nucl. Mater.* **204**, 65 (1993).
- [18] M. J. Alinger, G. R. Odette, and D. T. Hoelzer, *J. Nucl. Mater.* **329–333**, 382 (2004).
- [19] E. A. Marquis, *Appl. Phys. Lett.* **93**, 181904 (2008).
- [20] M. J. Alinger, G. R. Odette, and D. T. Hoelzer, *Acta Mater.* **57**, 392 (2009).
- [21] J. He, F. Wan, K. Sridharan, T. R. Allen, A. Certain, V. Shutthanandan, and Y. Q. Wu, *J. Nucl. Mater.* **455**, 41 (2014).
- [22] N. A. Bailey, E. Stergar, M. Toloczko, and P. Hosemann, *J. Nucl. Mater.* **459**, 225 (2015).
- [23] D. J. Larson, P. J. Maziasz, I.-S. Kim, and K. Miyahara, *Scr. Mater.* **44**, 359 (2001).
- [24] M. Ohnuma, J. Suzuki, S. Ohtsuka, S.-W. Kim, T. Kaito, M. Inoue, and H. Kitazawa, *Acta Mater.* **57**, 5571 (2009).
- [25] M. Ratti, D. Leuvrey, M. H. Mathon, and Y. de Carlan, *J. Nucl. Mater.* **386–388**, 540 (2009).
- [26] T. Okuda and M. Fujirawa, *J. Mater. Sci. Lett.* **14**, 1600 (1995).
- [27] C. L. Fu, M. Krčmar, G. S. Painter, and X.-Q. Chen, *Phys. Rev. Lett.* **99**, 225502 (2007).
- [28] Y. Jiang, J. R. Smith, and G. R. Odette, *Phys. Rev. B* **79**, 064103 (2009).
- [29] D. Murali, B. K. Panigrahi, M. C. Valsakumar, S. Chandra, C. S. Sundar, and B. Raj, *J. Nucl. Mater.* **403**, 113 (2010).

- [30] H. Zhao, C. L. Fu, M. Krčmar, and M. K. Miller, *Phys. Rev. B* **84**, 144115 (2011).
- [31] L. Barnard, G. R. Odette, I. Szlufarska, and D. Morgan, *Acta Mater.* **60**, 935 (2012).
- [32] T. Danielson, E. Tea, and C. Hin, *J. Nucl. Mater.* **477**, 215 (2016).
- [33] C. Hin, B. D. Wirth, and J. B. Neaton, *Phys. Rev. B* **80**, 134118 (2009).
- [34] C. Hin and B. D. Wirth, *J. Nucl. Mater.* **402**, 30 (2010).
- [35] P. Jegadeesan, D. Murali, B. K. Panigrahi, M. C. Valsakumar, and C. S. Sundar, *Int. J. Nanosci.* **10**, 973 (2011).
- [36] *Landolt-Bornstein, Numerical Data and Functional Relationships in Science and Technology, Group III: Crystal and Solid State Physics, Volume 26, Diffusion in Solid Metals and Alloys*, edited by H. Mehrer (Springer, Berlin, 1990).
- [37] M. Alinger, Ph.D. Thesis, University of Santa Barbara, CA, 2004.
- [38] M. Athenes and V. V. Bulatov, *Phys. Rev. Lett.* **113**, 230601 (2014).
- [39] J. L. Bocquet, C. Barouh, and C. C. Fu, [arXiv:1611.03230](https://arxiv.org/abs/1611.03230) [cond-mat.mtrl-sci] (2016).
- [40] E. W. Montroll, *J. Soc. Indust. App. Math.* **4**, 241 (1956).
- [41] D. Wolf, *Philos. Mag. A* **47**, 147 (1983).
- [42] J. Soler, E. Artacho, J. Gale, A. Garcia, J. Junquera, P. Ordejon, and D. Sanchez-Portal, *J. Phys.: Condens. Matter* **14**, 2745 (2002).
- [43] E. Meslin, C. C. Fu, A. Barbu, F. Gao, and F. Willaime, *Phys. Rev. B* **75**, 094303 (2007).
- [44] E. Martinez, O. Senninger, C.-C. Fu, and F. Soisson, *Phys. Rev. B* **86**, 224109 (2012).
- [45] E. Hayward and C. C. Fu, *Phys. Rev. B* **87**, 174103 (2013).
- [46] J. P. Perdew, K. Burke, and M. Ernzerhof, *Phys. Rev. Lett.* **77**, 3865 (1996).
- [47] M. Methfessel and A. T. Paxton, *Phys. Rev. B* **40**, 3616 (1989).
- [48] H. Jonsson, G. Mills, and K. W. Jacobsen, in *Classical and Quantum Dynamics in Condensed Phase Simulations* (World Scientific, Singapore, 1998), Chap. 16, pp. 385–404.
- [49] A. Krashennnikov, P. Lehtinen, A. Foster, and R. Nieminen, *Chem. Phys. Lett.* **418**, 132 (2006).
- [50] N. Juslin and K. Nordlund, *J. Nucl. Mater.* **382**, 143 (2008).
- [51] F. Djurabekova, L. Malerba, R. Pasianot, P. Olsson, and K. Nordlund, *Philos. Mag.* **90**, 2585 (2010).
- [52] D. Murali, B. K. Panigrahi, M. C. Valsakumar, and C. S. Sundar, *J. Nucl. Mater.* **419**, 208 (2011).
- [53] G. Lucas and R. Schaublin, *Nucl. Instrum. Methods Phys. Res. B* **267**, 3009 (2009).
- [54] C. W. He, M. F. Barthe, P. Desgardin, S. Akhmadaliev, M. Behar, and F. Jomard, *J. Nucl. Mater.* **455**, 398 (2014).
- [55] T. Schuler, C. Barouh, M. Nastar, and C.-C. Fu, *Phys. Rev. Lett.* **115**, 015501 (2015).
- [56] J. J. Burton, *Phys. Rev. B* **5**, 2948 (1972).